Coupled Systems Mechanics, *Vol. 8, No. 3 (2019) 273-287*
DOI: https://doi.org/10.12989/csm.2019.8.3.273

Residual stress in an elastoplastic annular disc interacting with an elastic inclusion

Somayeh Bagherinejad Zarandi[1], Hsiang-Wei Lai[1], Yun-Che Wang[*1] and Sergey M. Aizikovich[2]

[1]Department of Civil Engineering, National Cheng Kung University,
1 University Road, Tainan 70101, Taiwan
[2]Research and Education Center "Materials", Don State Technical University and
Vorovich Research Institute of Mechanics and Applied Mathematics,
Southern Federation University, Rostov-on-Don, Russia

(Received March 22, 2019, Revised April 12, 2019, Accepted April 13, 2019)

Abstract. Elastoplastic analysis of an annular disc, being fully constrained on its outer rim and interacting with a purely elastic inclusion perfectly bonded with its inner rim, is conducted to study its plastic deformation and residual stress under thermal cycles. The system is termed the composite disc. Quasi-static plane-strain deformation is assumed, and the von Mises yield criterion with or without the Ludwik hardening rule is adopted in our finite element calculations. Effects of multiple material properties simultaneously being temperature dependent on the plastic behavior of the composite disc are considered. Residual stress is analyzed from a complete loading and unloading cycle. Results are discussed for various inclusion radii. It is found that when temperature dependent material properties are considered, the maximum residual stress may be greater than the maximum stress inside the disc at the temperature-loaded state due to lower temperature having larger yield stress. Temperature independent material properties overestimate stresses inside materials, as well as the elastic irreversible temperature and plastic collapse temperature.

Keywords: plasticity; residual stress; temperature-dependent material properties; finite element analysis; composite circular disc

1. Introduction

Plasticity in the plane deformation is an important subject for scientific understanding and industrial applications. For examples, rigorous elastoplastic analysis of rotating annular disc has recently been carried out by Alexandrov *et al.* (2017) under the plane stress assumption. Studies of plastic deformation of bimetallic sheet under plane strain bending have been reported (Alexandrov *et al.* 2016). Furthermore, hollow discs with reversed yielding properties have recently been analyzed (Alexandrov *et al.* 2016). Since the abovementioned papers do not involve temperature loading, material properties are assumed to be constant throughout the analysis.

Plastic deformation of materials with the consideration of temperature dependent (TD) material

∗Corresponding author, Professor, E-mail: yunche@mail.ncku.edu.tw

http://www.techno-press.org/?journal=csm&subpage=8 ISSN: 2234-2184 (Print), 2234-2192 (Online)

properties is of importance for thermal loading in engineering analysis (Noda, 1970, Sayman and Arman 2006, Argeso and Eraslan 2008, Alexandrov *et al.* 2014, Alexandrov *et al.* 2014). Analytical results on discs in the two-dimensional analysis under thermal loading have shed new light, but no general analytical solutions have been provided (Alexandrov and Alexandrova 2001, Alexandrov and Chikanova 2000, Alexandrov *et al.* 2012). Effects of thickness variations on the elastoplastic behavior of annular discs have been studied (Wang *et al.* 2013). It was found that thickness variations have stronger effects when temperature-dependent material properties are considered. Aluminum composite discs under thermal loading have been studied (Topcu *et al.* 2008). However, in this reference, material properties are assumed to be temperature independent. Recently, studies on the composite disc in views of the two-dimensional and three-dimensional analysis under monotonic temperature loading with consideration of temperature dependent material properties have been recently reported (Zarandi *et al.* 2016).

Plastic deformation is known as one of important mechanisms to dissipate energy caused by external loading, albeit permanent deformation or residual stress may be present in the material when loads are removed. Wang and Ko (2015) reported the energy dissipation properties of a composite beam-column connector due to viscoelastic and plastic deformation processes. In addition to plasticity, materials' microstructures may give rise to unusual mechanical properties, such as negative Poisson's ratio (Wang *et al.* 2017). In addition, functionally graded materials have also demonstrated useful mechanical properties for industrial applications (Krenev *et al.* 2015).

In this work, we adopt the finite element method to numerically study the elastoplastic behavior and residual stress of the plane-strain composite disc under quasi-static temperature thermal loading and unloading. Both temperature dependent (TD) and temperature independent (TI) material properties are analyzed. Effects of hardening and inclusion size are considered. Our numerical results may serve as reference data for experimental findings or future analytical solutions on such problem.

2. Theoretical and numerical considerations

As shown in Fig. 1 (a), the composite disc consisting of a purely elastic inclusion and elastoplastic matrix. The inclusion-matrix interface is assumed to be perfectly bonded. The outer boundary of the composite disc is fully clamped, and a uniform temperature difference is

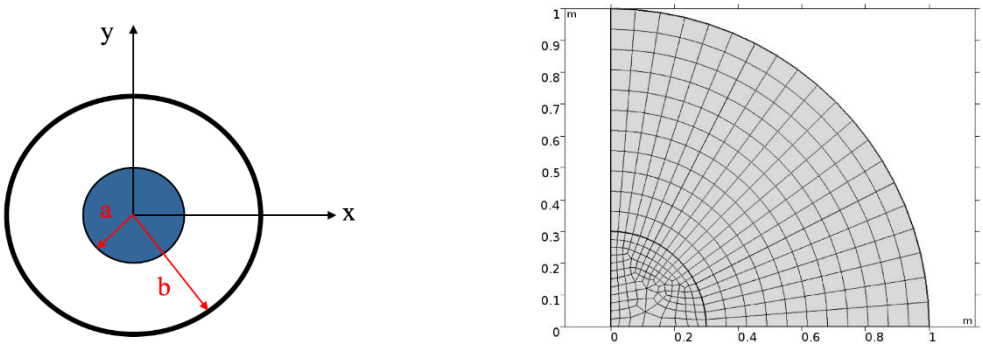

(a) Schematic of the composite disc (b) Typical finite element mesh

Fig. 1 Schematic and numerical mesh of the disc confined on the outer rim

applied to the whole disc under the quasi-static assumption. The physical properties of the purely elastic inclusion are assumed to be temperature independent, but those of the elastoplastic matrix are temperature dependent. In this work, the plane-strain assumptions are adopted, and the elastoplastic problems are analysed via the finite element method with the axisymmetric assumption.

For the elastic-perfectly plastic material model, the von Mises criterion is adopted in this work (Lubliner 1990).

$$F = \sigma_{mises} - \sigma_y, \tag{1}$$

Here the yield function is denoted by F, and the yield surface is described by F = 0. The von Mises stress is defined as follows in terms of deviatoric stress tensor s_{ij}, or its second invariant J_2.

$$\sigma_{mises} = \sqrt{3J_2(s_{ij})} = \sqrt{\frac{3}{2}s_{ij}s_{ij}} \quad \text{and} \quad s_{ij} = \sigma_{ij} - \frac{1}{3}\sigma_{kk}\delta_{ij}. \tag{2}$$

Here δ_{ij} is the Kronecker delta function, and the Einstein summation rule for the indices is applied. In addition, local effective plastic strain is defined as follows.

$$\dot{\varepsilon}_{pe} = \sqrt{\frac{2}{3}\dot{\varepsilon}^p_{ij}\dot{\varepsilon}^p_{ij}}, \tag{3}$$

As for the Ludwik hardening model, its stress is related to the effective plastic strain as follows

$$\sigma_y(\varepsilon_{pe}) = \sigma_{y0} + K\varepsilon^n_{pe}. \tag{4}$$

The hardening parameter K controls the hardening strength, and is assumed to be temperature dependent. The hardening coefficient is denoted by n, which is assumed to be temperature independent throughout this work. The effective plastic strain is denoted by ε_{pe}. It is noted that the Ludwik model may be reduced to the linear isotropic hardening model by setting n = 1, and

$$\frac{1}{K} = \frac{1}{E_T} - \frac{1}{E}, \tag{5}$$

where E_T is the isotropic tangent modulus and E the Young‘s modulus of the annular region of the composite disc.

The temperature-dependent material properties of the matrix are adopted from Seif *et al.* (2016) for yield stress $\sigma_y(T)$, Young’s modulus E(T) and hardening parameter K(T), as shown in Eqs. (6)-(8). These three temperature dependent functions are in units of Pa (N/m^2). It is assumed the matrix is a structural steel. We consider the matrix is elastic-perfectly plastic isotropic, homogeneous material with temperature-dependent properties. In addition, effects of hardening are also analysed with the Ludwik model (Hill, 1950). The symbols ν and α denote Poisson’s ratio and linear thermal expansion coefficient, respectively. Their temperature dependence, as shown in Eqs. (9) and (10), is based on Argeso and Eraslan (2008).

$$\sigma_y(T) = \sigma_0\left\{0.09 + 0.91e^{\left[-\frac{1}{2}\left(\frac{T-20}{588}\right)^{7.514} - \frac{T-20}{1352}\right]}\right\} \tag{6}$$

$$E(T) = E_0 e^{\left[-\frac{1}{2}\left(\frac{T-20}{639}\right)^{3.768} - \frac{T-20}{3300}\right]} \tag{7}$$

$$K(T) = K_0 e^{\left[-\left(\frac{T}{540}\right)^{7.82}\right]} \tag{8}$$

$$v(T) = v_0[1 + 2.5 \times 10^{-4}(T-20) - 2.5 \times 10^{-7}(T-20)^2] \tag{9}$$

$$\alpha(T) = \alpha_0[1 + 2.56 \times 10^{-4}(T-20) - 2.14 \times 10^{-7}(T-20)^2] \tag{10}$$

where the testing temperature T is in ˚C and reference temperature is 20˚C. Also, at the reference temperature, the Young's modulus, yield stress, Poisson's ratio and linear thermal expansion coefficient of the matrix material are assumed to be E_0 = 200 GPa, σ_0 = 410 MPa, v_0 = 0.3, and α_0 = 11.7x10^{-6} per ˚C, respectively. The reference hardening parameter is set to be $K0$ = 694.81 MPa (Seif *et al.*, 2016). Furthermore, we assume the Young's modulus of the inclusion E_i = 41 GPa, the inclusion Poisson's ratio v_i = 0.28, the inclusion linear thermal expansion coefficient α_i = 5.0 x 10^{-6}. This choice of inclusion material parameters is representative for the inclusion to provide elastic and thermal deformation to interact with the elastoplastic matrix. Deformation process is assumed to be quasi-static throughout this work.

A typical finite element mesh is shown in Fig. 1(b) with the inclusion radius a = 0.3 m and whole disc radius b = 1 m. In this work, three different inclusion radii are chosen, namely a = 0.1, 0.3 or 0.7. The value of *a* and *b* was so chosen for the purpose of examining the effects of thermal loading on the composite disc with different sizes of inclusion. The *a/b* ratio dominates elastically irreversible temperature (T_e) and plastic collapse temperature (T_p), as discussed with Figs. 5 and 6. The number of rectangular quadratic elements used in the analysis was about 20000, and the number of degrees of freedom (d.o.f.) was about 90000, including the d.o.f. for plasticity. We adopted COMSOL (2019) for the finite element calculations throughout this study.

3. Results and discussion

3.1 Temperature loading/unloading profile and temperature-dependent material properties

As an example, Fig. 2 (a) shows the quasi-static thermal loading and unloading profile, for ΔT = 100 K temperature difference, with respect to the loading parameter, which can be considered as a step size parameter during the analysis. In our calculated cases, ΔT is so chosen that plastic behavior can be observed. Furthermore, at a chosen loading parameter, say 1, temperature of 393 K is uniformly applied to the whole disc. Reference temperature is set to be T_{ref} = 293 K (i.e., 20˚C). Since only steady-state response of the composite disc to temperature is analyzed, dynamic effects, such as Biot number or thermal conductivity, are not considered.

We term "loading stage 1" for loading parameter = 0, which is the initial state; "loading stage 2" for loading parameter = 1, which is the maximum loaded state; "loading stage 3" for loading parameter = 2, which is the unloaded state and residual stress is determined at this stage of loading. At loading stage 1, T is 305˚C, and at loading stage 2, T = 395˚C. Since only static equilibrium is studied, the rate of temperature change does not affect the results of our analysis. The temperature functions for the material properties are shown in Fig. 2 (b). As can be seen, the yield stress exhibits strongest temperature dependence. Thermal expansion coefficients increase

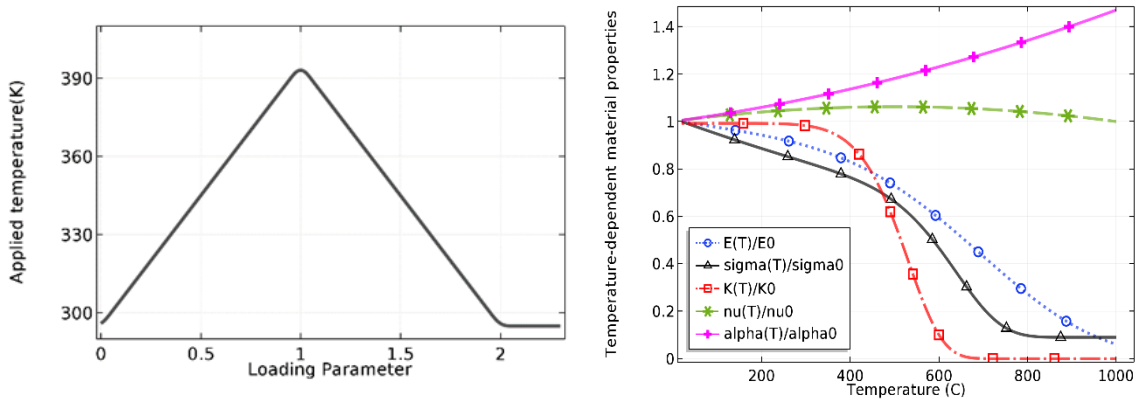

(a) Quasi-static thermal loading profile (b) Temperature-dependent material properties

Fig. 2 Temperature loading/unloading profile and temperature-dependent functions stated in Eqs. (7)-(10)

with temperature and Poisson's ratio is assumed to be mildly dependent on temperature. The other three material parameters, i.e., Young's modulus, yield stress and hardening parameter K, decrease with temperature.

3.2 Effects of material parameters being temperature dependent

At the loading stage 2, i.e., the composite disc under the largest temperature loading, the von Mises stress distributions inside the disc with the consideration of single material parameter changing with temperature are shown in Fig. 3(a). It can be seen that, except for the yield stress, results from other single TD parameter do not deviate from the temperature independent (TI) case. When considering multiple TD material parameters, one can see the TD material parameters other than yield stress contribute little to the stress distribution. It is noted that, in Figs. 3-9, the horizontal axis is in units of meter. However, since we choose the outer radius always equal to 1 m, the numeric values of the radius abscissa can also be interpreted as the radius ratio of inclusion to the matrix.

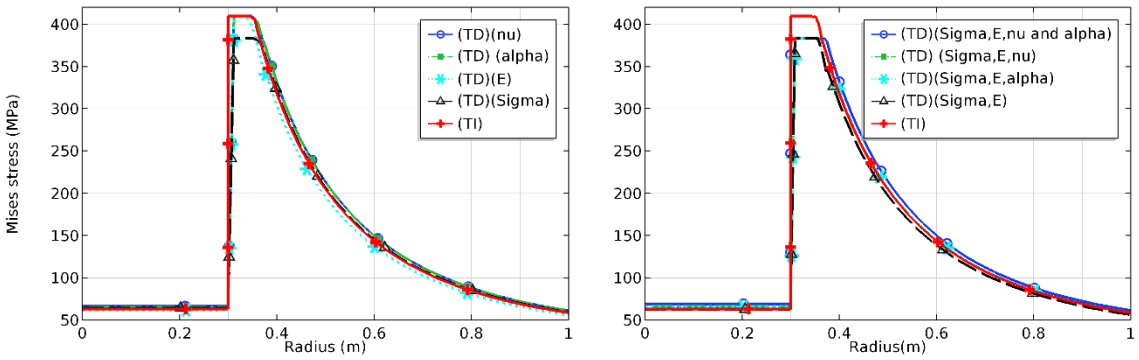

(a) Effects of single TD material parameter (b) Effects of multiple TD material parameters

Fig. 3 Effects of material parameters being temperature-dependent at the loading stage 2 for $\Delta T = 100$ K

3.3 Effects of radius ratio on residual stress

With the perfectly plastic assumption, residual Mises stress distributions (red color) obtained from the loading stage 3 for radius ratio a/b = 0.1, 0.3 and 0.7 are shown in Fig. 4(a)-4(c),

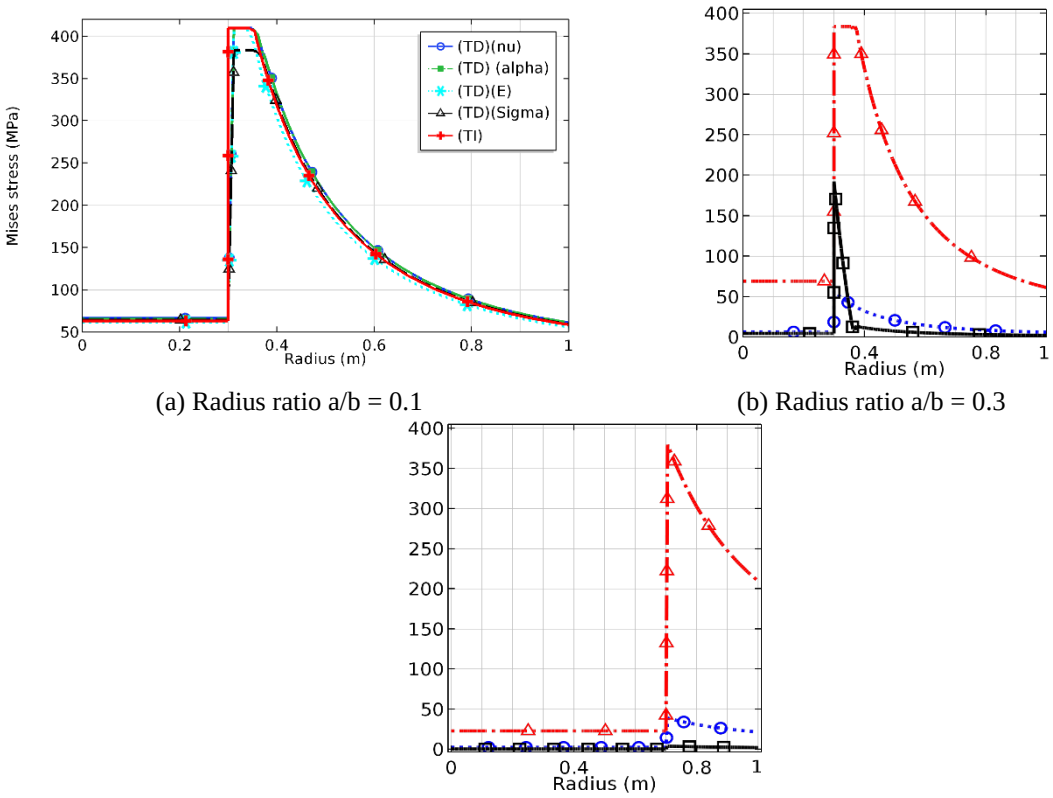

(a) Radius ratio a/b = 0.1 (b) Radius ratio a/b = 0.3

(c) Radius ratio a/b = 0.7

Fig. 4 Residual stress distribution, i.e., at the loading stage 3, for various radius ratios under ΔT = 100 K

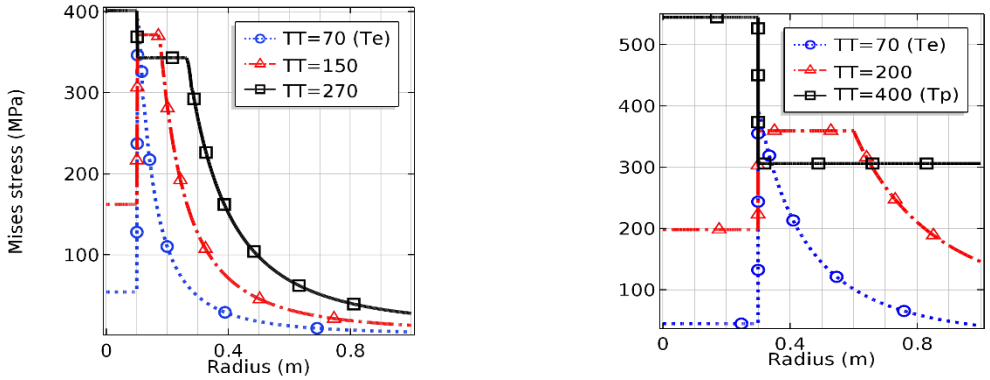

(a) Radius ratio a/b = 0.1 (b) Radius ratio a/b = 0.3

Fig. 5 Stress distribution, i.e., at loading stage 2, under various thermal loadings for the TD cases

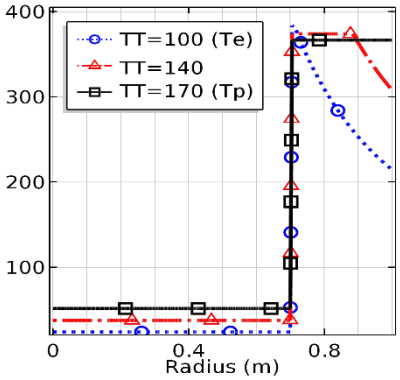

(c) Radius ratio a/b = 0.7

Fig. 5 Continued

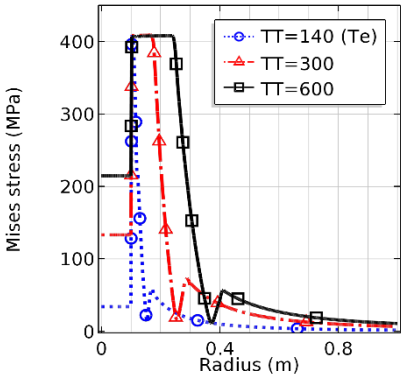

(a) Radius ratio a/b = 0.1

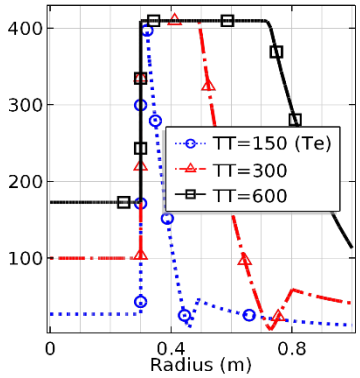

(b) Radius ratio a/b = 0.3

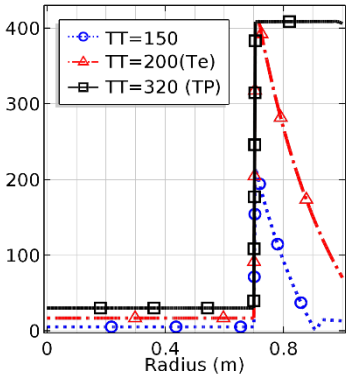

(c) Radius ratio a/b = 0.7

Fig. 6 Residual stress distribution, i.e., at loading stage 3, under various thermal loadings for the TD cases

respectively. In order to compare with the initial (stage 1) and maximum (stage 2) stress distribution.

To compare effects of different temperatures with the consideration of temperature dependent (TD) material properties, Figs. 5 and 6 show the Mises stress and Mises residual stress

distributions at selected temperatures. The label TT in figure legends throughout this paper has the same meaning as ΔT. In addition, the labels Te and Tp indicate the elastic reversible temperature and plastic collapse temperature, respectively. The method used to determine Te and Tp numerically in this work is by gradually increasing ΔT and observing the Mises stress plateau

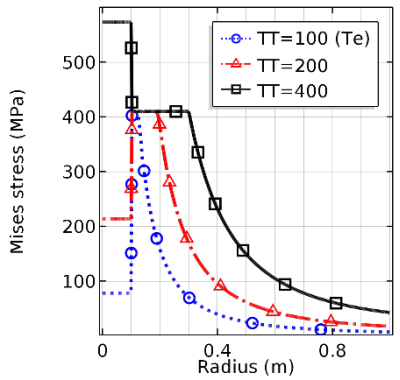

(a) Radius ratio a/b = 0.1

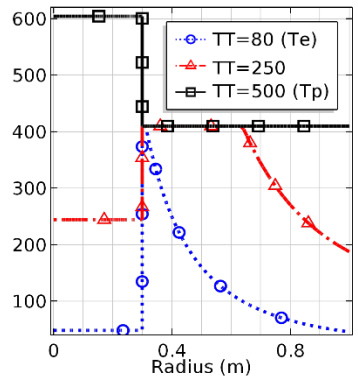

(b) Radius ratio a/b = 0.3

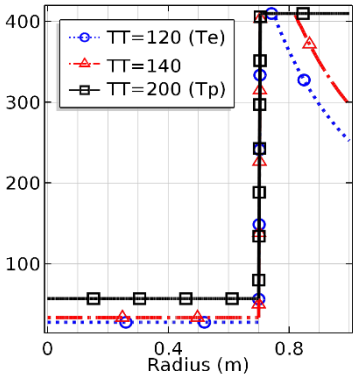

(c) Radius ratio a/b = 0.7

Fig. 7 Stress distribution, i.e., at loading stage 2, under various thermal loadings for the TI cases

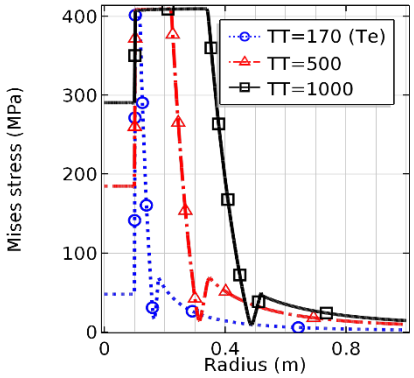

(a) Radius ratio a/b = 0.1

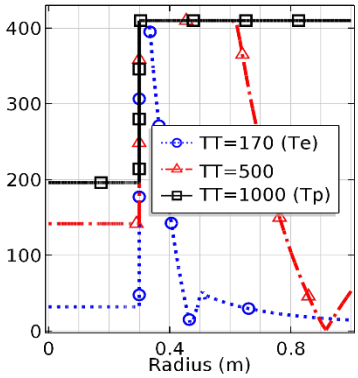

(b) Radius ratio a/b = 0.3

Fig. 8 Residual stress distribution, i.e., at loading stage 3, under various thermal loadings for the TI cases

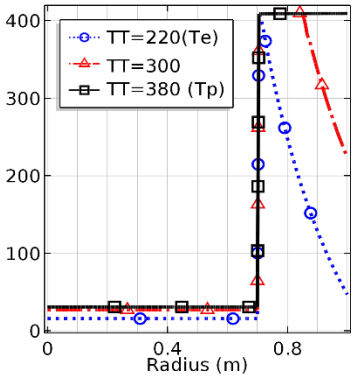

(c) Radius ratio a/b = 0.7

Fig. 8 Continued

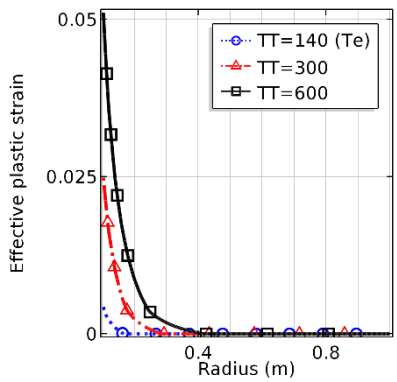

(a) Radius ratio a/b = 0.1

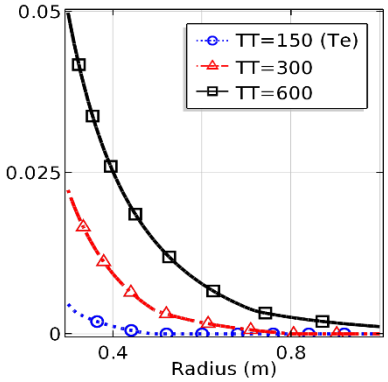

(b) Radius ratio a/b = 0.3

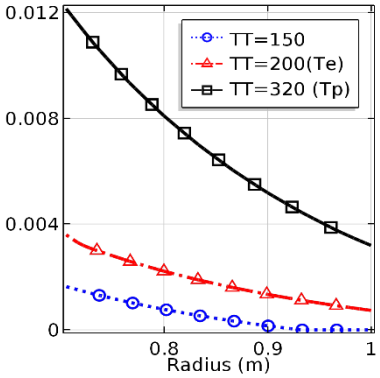

(c) Radius ratio a/b = 0.7

Fig. 9 Effective plastic strain for various three radius ratios under various temperature loading

in the figures at loading stage 2. If the stress plateau is just formed near the inclusion-matrix boundary, then the corresponding temperature is termed Te. If the stress plateau is in the entire matrix domain, then the corresponding temperature is called Tp. From the figures, it can be seen that these two temperatures are highly dependent on the a/b ratio. For the a/b = 0.3 and 0.7 cases,

the plastic collapse temperature can be determined, while the Tp for the a/b = 0.1 case requires much higher temperature than ΔT = 270 K. As for the residual stress, the dips shown in the residual stress curves are the consequence of self-equilibration to maintain equilibrium under no external excitations.

Contrast to the cases shown in Figs. 5 and 6 with TD material parameters, Figs. 7 and 8 show the Mises stress and Mises residual stress for the cases of material properties being temperature independent. As can be seen, although the distribution patterns are similar, the TI cases overestimate stresses inside the disc, as well as the T_e and T_p temperature. For the a/b =0.3 and 0.7 case, it can be seen that the TI models always overestimate T_e and T_p temperature, while the TD models reveal smaller temperature values for onset of elastic irreversibility and plastic collapse. It is noted that the maximum residual stress is greater than the maximum stress at loading stage 2 due to larger yield stress at lower temperature. For the TI case, this phenomenon does not occur, and the maximum stresses are always the same at any loading stage.

3.4 Plastic strain after unloading

The effective plastic strains in the Mises sense in the matrix after unloading are shown in Fig. 9 for various loading history. Note since the inclusion is assumed to be purely elastic, the horizontal axis of the figures starts from different values in accordance with the size of the inclusion. As can be seen, the maximum effective plastic strain is about 5% for the a/b = 0.1 and 0.3 case. However, the maximum plastic strain is only about 1.2% for the a/b = 0.7 case at the temperature difference ΔT = 320 K.

3.5 Effects of hardening rules

With the temperature dependent parameter K(T), shown in Eq. (8), and temperature independent coefficient *n*, used in Eq. (4), in the Ludwik model, we compare the Mises stress at the loading stage 2 and residual stress distributions in Fig. 10 and 11, respectively. The applied temperature difference was ΔT = 200 K. As can be seen in Fig. 10, regardless hardening, temperature independent cases always overestimate stress levels in the stress plastic deformed regime. However, in the region between elastic-plastic boundary and outer rim of the disc, the disc only deforms elastically, the difference between TI and TD with or without hardening is small.

As for the residual stresses shown in Fig. 11, when a/b = 0.1, the differences between data with and without hardening are small for both the TD and TI case. However, the differences become noticeable for a/b = 0.3 and a/b= 0.7. Due to the temperature dependence, the yield stress is larger at low temperatures. Hence, the residual stress is larger than that calculated from the TI models.

From our analysis, it can be seen that the a/b ratio plays a crucial role in stress distribution and T_e and T_p temperatures. In general, T_e and T_p are larger when a/b is small. At the same temperature loading, larger a/b ratio leads to smaller residual stress at the interface. One may control residual stress by selecting suitable a/b ratios. In addition, one may introduce a buffer layer, which may be functionally graded, between the inclusion and matrix to reduce its magnitude. Detailed design of the buffer layer requires further analysis.

3.6 Discussions on other stress components

In the previous sections, discussions based on the Mises stress are made. Here, we demonstrate

other residual stress components for the a=0.3, TD case without hardening effects. The hydrostatic residual stress, defined by $(\sigma_{xx}+\sigma_{yy}+\sigma_{zz})/3$, is shown in Fig. 12 (a). Due to the axisymmetric nature

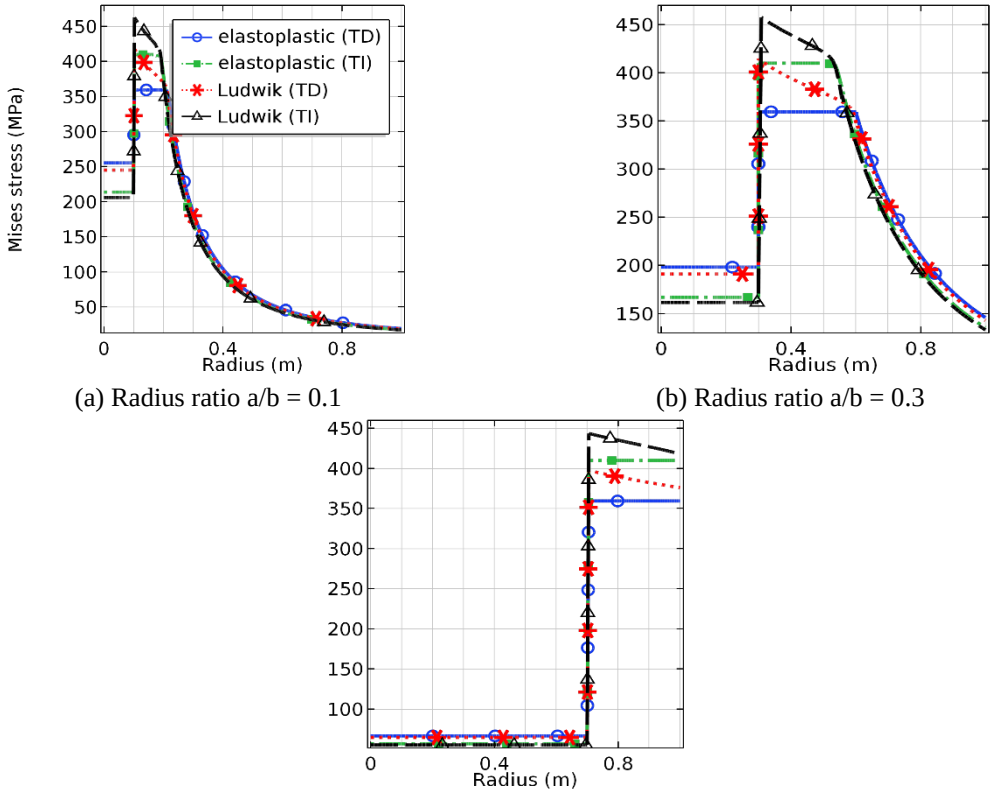

(a) Radius ratio a/b = 0.1 (b) Radius ratio a/b = 0.3

(c) Radius ratio a/b = 0.7

Fig. 10 Effects of hardening rules on the Mises stress under thermal loading ΔT = 200 K at the loading stage 2

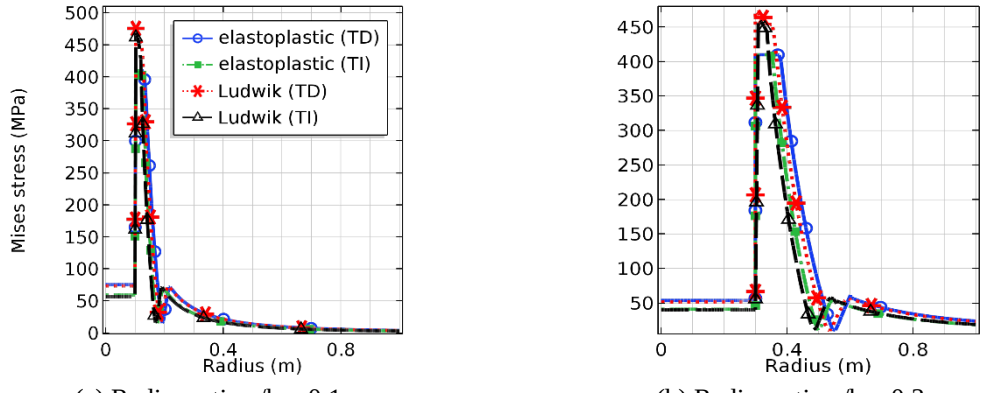

(a) Radius ratio a/b = 0.1 (b) Radius ratio a/b = 0.3

Fig. 11 Effects of hardening rules on residual stress under thermal loading ΔT = 200 K at the loading stage 3

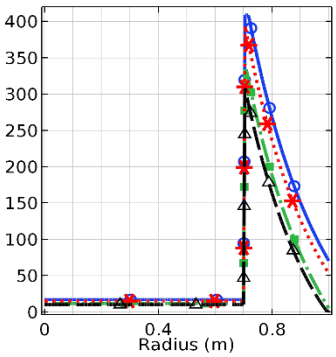

(c) Radius ratio a/b = 0.7

Fig. 11 Continued

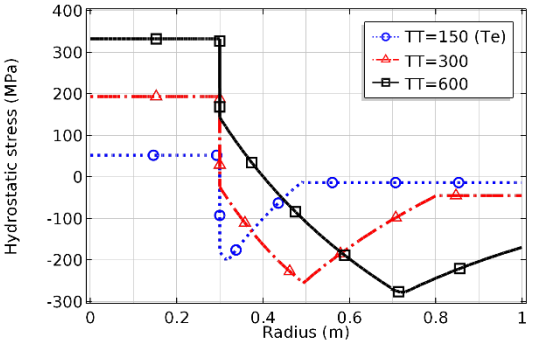

(a) Residual $\sigma_{kk}/3$ distribution along y-axis

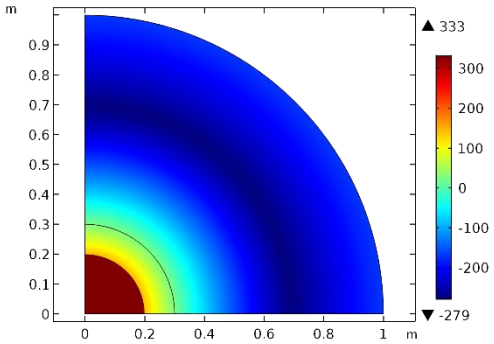

(b) Residual $\sigma_{kk}/3$ distribution for $\Delta T = 600$ K

Fig. 12 Distribution of hydrostatic residual stress ($\sigma_{kk}/3$) under various maximum thermal loading

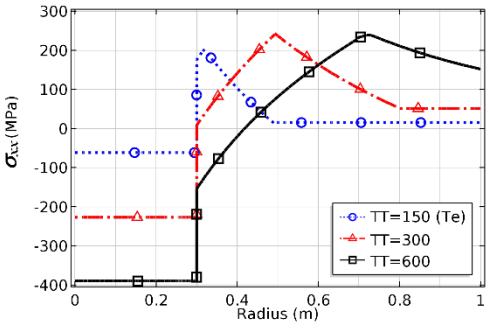

(a) Residual σ_{xx} distribution along radial axis

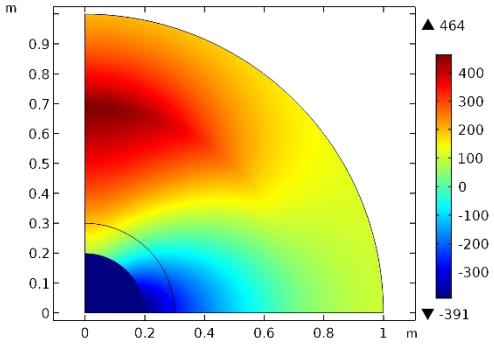

(b) Residual σ_{xx} distribution for $\Delta T = 600$ K

Fig. 13 Distribution of σ_{xx} residual stress under various maximum thermal loading

of the problem, the hydrostatic stress contour under $\Delta T = 600$ K, shown in Fig. 12 (b), does not exhibit any θ dependence. In the contour plots, the color bars are in units of MPa. At elevated temperature, thermal expansion of the matrix is greater than that of the inclusion.

Hence, the size of the inclusion is reduced. For the same case, its σ_{xx}, σ_{xy} and σ_{zz} residual stress distributions are shown in Figs. 13, 14 and 15, respectively. It can be seen that the residual stress

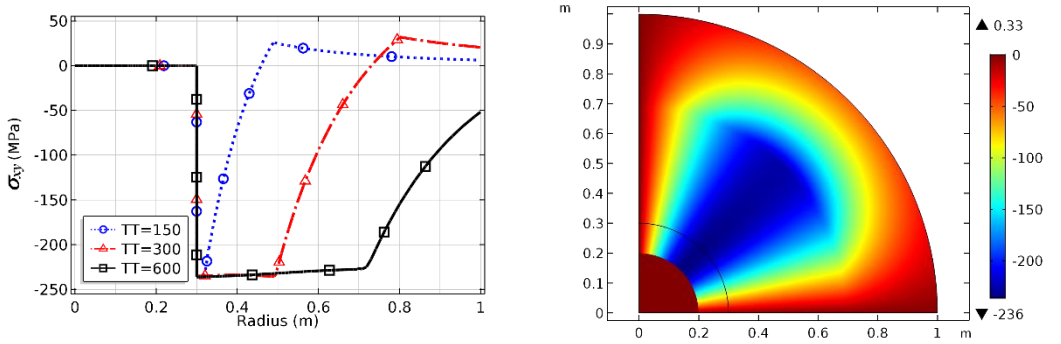

(a) Residual σ_{xy} distribution along radial axis (b) Residual σ_{xy} distribution for ΔT = 600 K

Fig. 14 Distribution of σ_{xy} residual stress under various maximum thermal loading

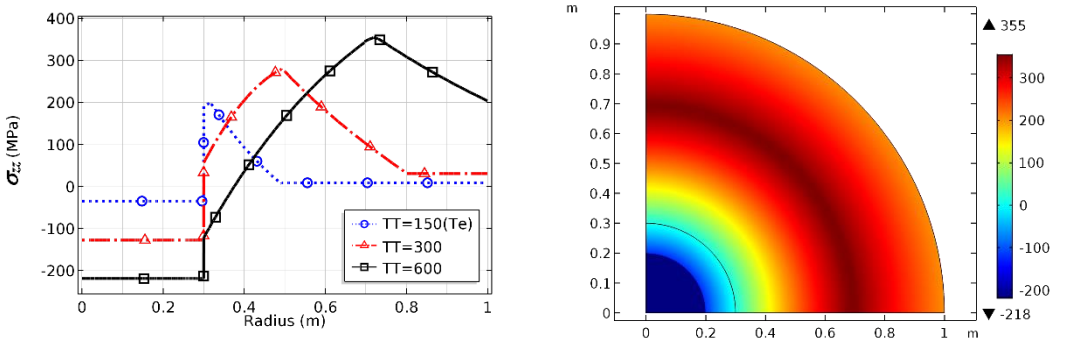

(a) Residual σ_{zz} distribution along radial axis (b) Residual σ_{zz} distribution for ΔT = 600 K

Fig. 15 Distribution of σ_{zz} residual stress under various maximum thermal loading

σ_{zz} has no θ dependence, while σ_{xx}, and σ_{xy} are dependent on θ., following the transformation rule of second order tensor. The distributions of residual stress satisfy the self equilibrium condition.

In the above quasi-static analysis, since the interface between the inclusion and matrix is assumed to be perfectly bonded, the nature of discontinuity due to mismatch in material constants at the interface causes stress jumps around it, as can be seen in Figs. 12-15. Because the dynamic effects are not included in the present analysis, our qualitative numerical results may be considered as realistic under the presumptions of steady-state responses and perfect bonding at the interface. As for possible real-life applications, our analysis may be used to delineate the residual stress in machine parts under thermal loading. Furthermore, the numerical results may serve as reference data to compare future experimental data or analytical solutions.

4. Conclusions

Elastoplastic behavior and residual stress of the composite disc under thermal loading and unloading are studied. Considerations of temperature-dependent material properties are of paramount importance in providing accurate estimations of stress distribution and plastic collapse temperature. Temperature-independent material properties overestimate stresses inside the material, as well as T_e and T_p. It is found that, for the TD models, maximum residual stress may be

greater than their maximum stress at the loaded stage since at high temperature the yield stress is smaller than that at low temperature.

Acknowledgments

Funding from Taiwan Ministry of Science and Technology under the contract number of NSC 107-2221-E-006-028 is gratefully appreciated. This research was, in part, supported by the Ministry of Education, Taiwan, R.O.C, and the Aim for the Top University Project to the National Cheng Kung University (NCKU). We are also grateful to the National Center for High-performance Computing for computer time and facilities.

References

Alexandrov, S. and Alexandrova, N. (2001), "Thermal effects on the development of plastic zones in thin axisymmetric plates", *J. Strain Anal. Eng. Des.*, **36**(2), 169-175. https://doi.org/10.1243%2F0309324011512720.

Alexandrov, S. and Chikanova, N. (2000), "Elastic-plastic stress-strain state of a plate with a pressed-in inclusion in thermal field", *Mech. Solids*, **35**, 125-132.

Alexandrov, S., Chung, K. and Jeong, W. (2018), "Stress and strain fields in rotating elastic/plastic annular disks of pressure-dependent material", *Mech. Based Des. Struct. Machines*, **46**(3), 318-332. https://doi.org/10.1080/15397734.2017.1342095.

Alexandrov, S., Wang, Y.C. and Aizikovich, S. (2014), "Effect of temperature-dependent mechanical properties on plastic collapse of thin discs", *J. Mech. Eng. Sci. Part C*, **228**(14), 2483-2487. https://doi.org/10.1177%2F0954406213519757.

Alexandrov, S., Wang, Y.C. and Jeng, Y.R. (2014), "Elastic-plastic stresses and strains in thin discs with temperature-dependent properties subject to thermal loading", *J. Therm. Stresses*, **37**(4), 488-505. https://doi.org/10.1080/01495739.2013.870864.

Alexandrov, S.E., Kien, N.D., Manh, D.V. and Grechnikov, F.V. (2016), "Plane strain bending of a bimetallic sheet at large strains", *Struct. Eng. Mech.*, **58**(4), 641-659. https://doi.org/10.12989/sem.2016.58.4.641.

Alexandrov, S.E., Lomakin, E.V. and Jeng, Y.R. (2012), "Solution of the thermoelasticplastic problem for a thin disk of plastically compressible material subject to thermal loading", *Dokl. Phys.*, **57**(3), 136-139. https://doi.org/10.1134/S1028335812030081.

Alexandrov, S.E., Pirumov, A.R. and Jeng, Y.R. (2016), "Description of reversed yielding in thin hollow discs subject to external pressure", *Struct. Eng. Mech.*, **58**(4), 661-676. https://doi.org/10.12989/sem.2016.58.4.661.

Argeso, H. and Eraslan, A.N. (2008), "On the use of temperature-dependent physical properties in thermomechanical calculations for solid and hollow cylinders", *Int. J. Thermal Sci.*, **47**(2), 136-146. https://doi.org/10.1016/j.ijthermalsci.2007.01.029.

COMSOL (2019), www.comsol.com.

Hill, R. (1950), *The Mathematical Theory of Plasticity*, Oxford University Press Inc., New York, U.S.A.

Krenev, L.I., Aizikovich, S.M., Tokovyy, Y.V. and Wang, Y.C. (2015), "Axisymmetric problem on the indentation of a hot circular punch into an arbitrarily nonhomogeneous half-space", *Int. J. Solids Struct.*, **59**, 18-28. https://doi.org/10.1016/j.ijsolstr.2014.12.017.

Lubliner, J. (1990), *Plasticity Theory*, Macmillan Publishing Company, New York, U.S.A.

Noda, N. (1991), "Thermal stresses in materials with temperature-dependent properties," *Appl. Mech. Rev.*, **44**(9), 383-397. https://doi.org/10.1115/1.3119511.

Sayman, O. and Arman, Y. (2006), "Thermal stresses in a thermoplastic composite disc under a steady state temperature distribution", *J. Rein. Plas. Compos.*, **25**(16), 1709-1722. https://doi.org/10.1177%2F0731684406068416.

Seif, M., Main, J., Weigand, J., Sadek, F., Choe, L., Zhang, C., Gross, J., Luecke, W. and McColskey, D. (2016), "Temperature-dependent material modeling for structural steels: Formulation and application", NIST Technical Note 1907, US Department of Commerce, National Institute of Standards and Technology.

Topcu, M., Altan, G., Callioglu, H. and Altan, B.D. (2008), "Thermal elastic-plastic analysis of an aluminium composite disc under linearly decreasing thermal loading", *Adv. Compos. Lett.*, **17**(3), 87-96. https://doi.org/10.1177%2F096369350801700302.

Wang, Y.C. and Ko, C.C. (2015), "Energy dissipation of steel-polymer composite beam-column connector", *Steel Compos. Struct.*, **18**(5), 1161-1176. https://doi.org/10.12989/scs.2015.18.5.1161.

Wang, Y.C., Alexandrov, S. and Jeng, Y.R. (2013), "Effects of thickness variations on the thermal elastoplastic behavior of annular discs", *Struct. Eng. Mech.*, **47**(6), 839-856. https://doi.org/10.12989/sem.2013.47.6.839.

Wang, Y.C., Shen, M.W. and Liao, S.M. (2017), "Microstructural effects on the Poisson's ratio of star-shape two-dimensional systems", *Physica Status Solidi B*, **254**(12), 1700024. https://doi.org/10.1002/pssb.201700024.

Zarandi, S.B., Wang, Y.C. and Novozhilova, O.V. (2016), "Plastic behavior of circular discs with temperature-dependent properties containing an elastic inclusion", *Struct. Eng. Mech.*, **58**(4), 731-743. https://doi.org/10.12989/sem.2016.58.4.731.

DC